nature chemistry

ARTICLES

PUBLISHED ONLINE: 17 NOVEMBER 2013 | DOI: 10.1038/NCHEM.1802

# Self-healing chemistry enables the stable operation of silicon microparticle anodes for high-energy lithium-ion batteries

Chao Wang[1†], Hui Wu[2,3†], Zheng Chen[1], Matthew T. McDowell[2], Yi Cui[2,4*] and Zhenan Bao[1*]

**The ability to repair damage spontaneously, which is termed self-healing, is an important survival feature in nature because it increases the lifetime of most living creatures. This feature is highly desirable for rechargeable batteries because the lifetime of high-capacity electrodes, such as silicon anodes, is shortened by mechanical fractures generated during the cycling process. Here, inspired by nature, we apply self-healing chemistry to silicon microparticle (SiMP) anodes to overcome their short cycle-life. We show that anodes made from low-cost SiMPs (~3–8 μm), for which stable deep galvanostatic cycling was previously impossible, can now have an excellent cycle life when coated with a self-healing polymer. We attain a cycle life ten times longer than state-of-art anodes made from SiMPs and still retain a high capacity (up to ~3,000 mA h $g^{-1}$). Cracks and damage in the coating during cycling can be healed spontaneously by the randomly branched hydrogen-bonding polymer used.**

When faced with the dilemma of mechanical fractures in biological systems, nature offers a smart solution: self-healing. Soft biomaterials, such as human skin, have the ability to self-heal or self-repair when damaged[1]. After wounds heal, the skin is able to retain sensing functionalities. The ability to self-heal after mechanical damage has enhanced significantly the lifetime of biomaterials. In a similar vein, synthetic self-healing polymers (SHPs) are able to repair themselves and recover functionalities despite being subjected to mechanical damage[2–8]. Recently, self-healing chemistry has been demonstrated to have exciting applications towards functional surfaces[9,10], electrical conductors[11–14] and electronic skin[8] with enhanced lifetime and durability.

The self-healing feature is particularly desirable for energy storage because the lifetimes of many rechargeable batteries are limited by the similar dilemma of mechanical fractures over the cycling process. Electrochemical reactions in battery materials normally result in structural changes, which may cause degradation and damage, and ultimately cause the battery to be non-functional with cycling[15–18]. Next-generation electrode materials for lithium-ion batteries are especially susceptible to these failure mechanisms because they react with greater amounts of lithium and thus undergo more drastic structural changes[16,19–23]. For example, silicon, which has a theoretical specific capacity ten times higher than that of conventional graphite anodes, usually suffers from fast capacity decay and short cycle-life. This is mainly because silicon expands volumetrically by up to three times on full lithium insertion (lithiation) and contracts significantly on lithium extraction (delithiation). These extreme volumetric changes can cause cracking and pulverization in the electrode, which lead to loss of electrical contact and excessive solid–electrolyte interphase (SEI) growth[15,24,25]. Even when incorporating the silicon materials with metal alloys or high-modulus polymer binders, mechanical fractures and damages still occur.

One feasible approach to increase the lifetime of silicon anodes is to use nanoscale silicon materials[26–30]. However, silicon nanoparticles (SiNPs) are only available in small quantities[31,32], but other nanostructured silicon materials, such as nanowires, nanospheres, nanotubes and nanocrystals, require chemical vapour deposition and/or template growth, all of which are difficult and expensive to scale up[26–29,33]. Therefore, silicon microparticles (SiMPs) are more promising as electrode materials towards practical industrial applications because they are cheap and readily commercially available. In addition, the use of SiMPs leads to higher volumetric energy density when compared to SiNPs. Obrovac and Krause demonstrated an effective approach to achieve high cycling stability of SiMP electrodes by controlling precisely the lithiation potential. This is a very promising strategy to achieve a high-energy electrode for lithium-ion batteries[34,35]. Recently, Chevrier and co-workers showed that microsize silicon alloy particles can have excellent charge–discharge cycling stability at certain conditions[36,37]. However, all previously reported pure SiMP anodes have an extremely short cycle-life over deep galvanostatic cycling[24]: the capacity rapidly drops to <80% of the initial value in less than ten cycles because of the significant fracture and particle detachment in the electrodes[38–41]. To overcome this challenge, others have used nanostructured SiMPs[42], but again the issues for scaling up remain. Here, we use a chemical approach to improve the cycling lifetime by coating the microparticles with a thin layer of hydrogen-bond-directed SHP. Compared with traditional polymer binders, the self-healing chemistry is designed to enable spontaneous repair of the mechanical damage in the electrode and thus increase the lifetime of the SiMP anode.

Figure 1a shows a schematic design of the self-healing electrode. In a traditional silicon-based anode, the polymer binder surrounds the silicon particles and binds the active materials to the current collector to maintain electrical contact (Fig. 1a, Scheme 1). On cycling, the stress generated by the huge volumetric changes

[1]Department of Chemical Engineering, Stanford University, California 94305, USA, [2]Department of Materials Science and Engineering, Stanford University, California 94305, USA, [3]State Key Laboratory of New Ceramics and Fine Processing, School of Materials Science and Engineering, Tsinghua University, Beijing 100084, China, [4]Stanford Institute for Materials and Energy Sciences, SLAC National Accelerator Laboratory, Menlo Park, California 94205, USA, †These authors contributed equally to this work. *e-mail: zbao@stanford.edu; yicui@stanford.edu

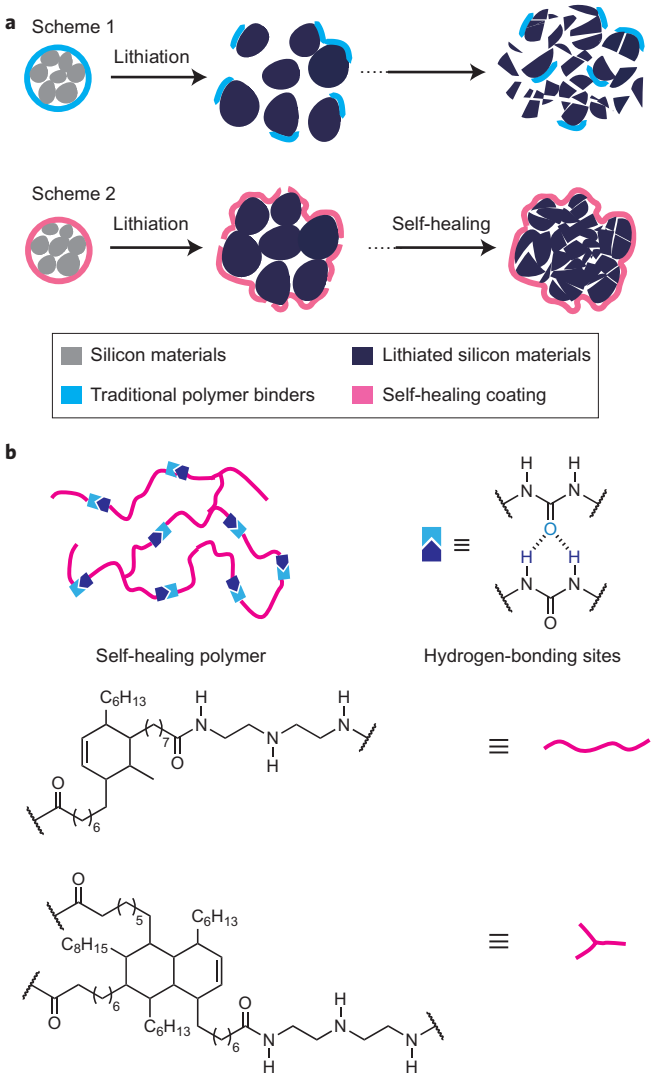


**Figure 1 | Design and structure of the self-healing electrode. a**, Scheme 1: schematic illustration of the design and behaviour of a conventional silicon electrode that shows failure of the electrode because of cracking in particles and polymer binder, which results in loss of electrical contact. Scheme 2: schematic illustration of the design and behaviour of our stretchable self-healing electrode that shows the maintaining of electrical contact between the broken particles and no cracks in the polymer binder because of the stretchability and incorporation of self-healing chemistry. **b**, Chemical structure of the SHP. Magenta lines, polymer backbones; light-blue and dark-blue boxes, hydrogen-bonding sites.

during the lithiation/delithiation of SiMPs causes fracture in the particles and polymer layers, resulting in loss of electrical contact and subsequent loss of capacity. In our current design (Fig. 1a, Scheme 2), the silicon electrode is coated with a thin layer of soft SHP. Different from conventional polymer binders, our SHP is stretchable and can repair spontaneously the mechanical damage and cracks in the electrode, which results in more stable mechanical and electrical connections among the silicon particles.

## Results and discussions

**Material design and characterizations.** There are two major categories of SHPs: (1) polymers with dynamic bonds[1,3,5] and (2) polymers embedded with microencapsulated healing agents[2]. For battery applications, a SHP based on dynamic bonding is more desirable because of its repeatable healing capability. Particularly, a hydrogen-bonding-directed[43] SHP is most advantageous as the coating layer as it allows for the cracks to heal autonomously and repeatedly at room temperature[6]. In addition, the SHP binder needs to be have a modest conductivity (>0.1 S cm$^{-1}$). We therefore designed a conductive composite of SHPs and conductive carbon black nanoparticles (CB). The SHP is a randomly branched hydrogen-bonding polymer, synthesized and fabricated using an approach modified from previous reports[5,6,44]. Its molecular structure is shown in Fig. 1b. We designed the polymer to have an amorphous structure with a low glass-transition temperature ($T_g$). If there is a crack or mechanical damage, the amorphous structure and low $T_g$ of the SHP allow the polymer chains at the fractured interfaces to rearrange, approach and intermix. This process is driven by the dynamic reassociation of hydrogen bonds at room temperature and leads to spontaneous self-healing. Indeed, the amorphous nature of the polymer was confirmed by differential scanning calorimetry (DSC), as evidenced by the lack of a melting-point peak over the whole temperature range (Fig. 2a). The DSC trace also confirms that $T_g$ is around 0 °C, much lower than room temperature. The SHP is made conductive (~0.25 S cm$^{-1}$) by uniformly dispersing CB into the polymer. The composite undergoes simultaneous mechanical and electrical self-healing at room temperature (Supplementary Figs 2–5). The self-healing capability is demonstrated in Fig. 2b, which shows that, after an electrical circuit is broken, when the two pieces of SHP acting as the conductors are brought together the circuit is completed in about one minute, and the light-emitting diode (LED) illuminates again. At the same time, the composite can withstand mechanical bending at the healed location, which indicates the quick electrical and mechanical healing at room temperature.

The crosslinked network of our SHP enables good mechanical stretchability as well, which allows the polymer to accommodate potential expansion of silicon to avoid non-healable damage, for example large cracks or delamination. As shown in Fig. 2c, our SHP can be stretched to three times its initial length without breaking (Supplementary Fig. 7). In comparison, traditional binders show much lower stretchability. Polyvinylidene fluoride (PVDF), sodium carboxymethyl cellulose (CMC) and alginate samples with similar sizes can be stretched only by up to 10%, 4% and 2%, respectively. Moreover, the SHP/CB composite retains its electrical conductivity during stretching. As shown in Fig. 2d, the resistance of the composite coated on polydimethylsiloxane did not change significantly as the composite was subjected to a 100% strain. The resistance remained within the same order of magnitude when subjected to >120 stretching cycles (Supplementary Fig. 8). This electromechanical durability also exists during expansion and shrinkage. We used an inflatable balloon coated with SHP/CB composite (Fig. 2e) to mimic the volumetric changes of silicon particles that took place during the lithiation/delithiation process. The conductivity of the composite coating changed from 0.25 S cm$^{-1}$ to 0.14 S cm$^{-1}$ on a volume expansion of about ten times, and the conductivity remained at 0.05 S cm$^{-1}$ even at the larger volume expansion of 25 times. On deflation, the conductivity was observed to revert close to the initial value.

**Battery testing.** Next, we proceeded to fabricate the self-healing silicon electrodes by sealing SiMPs inside a SHP/CB composite coating (see Methods for the detailed fabrication process). Coin cells with metallic lithium counter electrodes were employed to evaluate the electrochemical performance of the electrodes. On deep galvanostatic cycling between 0.01 and 1 V, the discharge (delithiation) capacity reached 2,617 mA h g$^{-1}$ for the first cycle at a current density of 0.4 A g$^{-1}$ (Fig. 3a,b), which is about six times higher than the theoretical capacity of graphite. The electrode shows good cycling stability: the discharge capacity retention was 100%, 95% and 80% after 20, 50 and 90 cycles, respectively. This is in

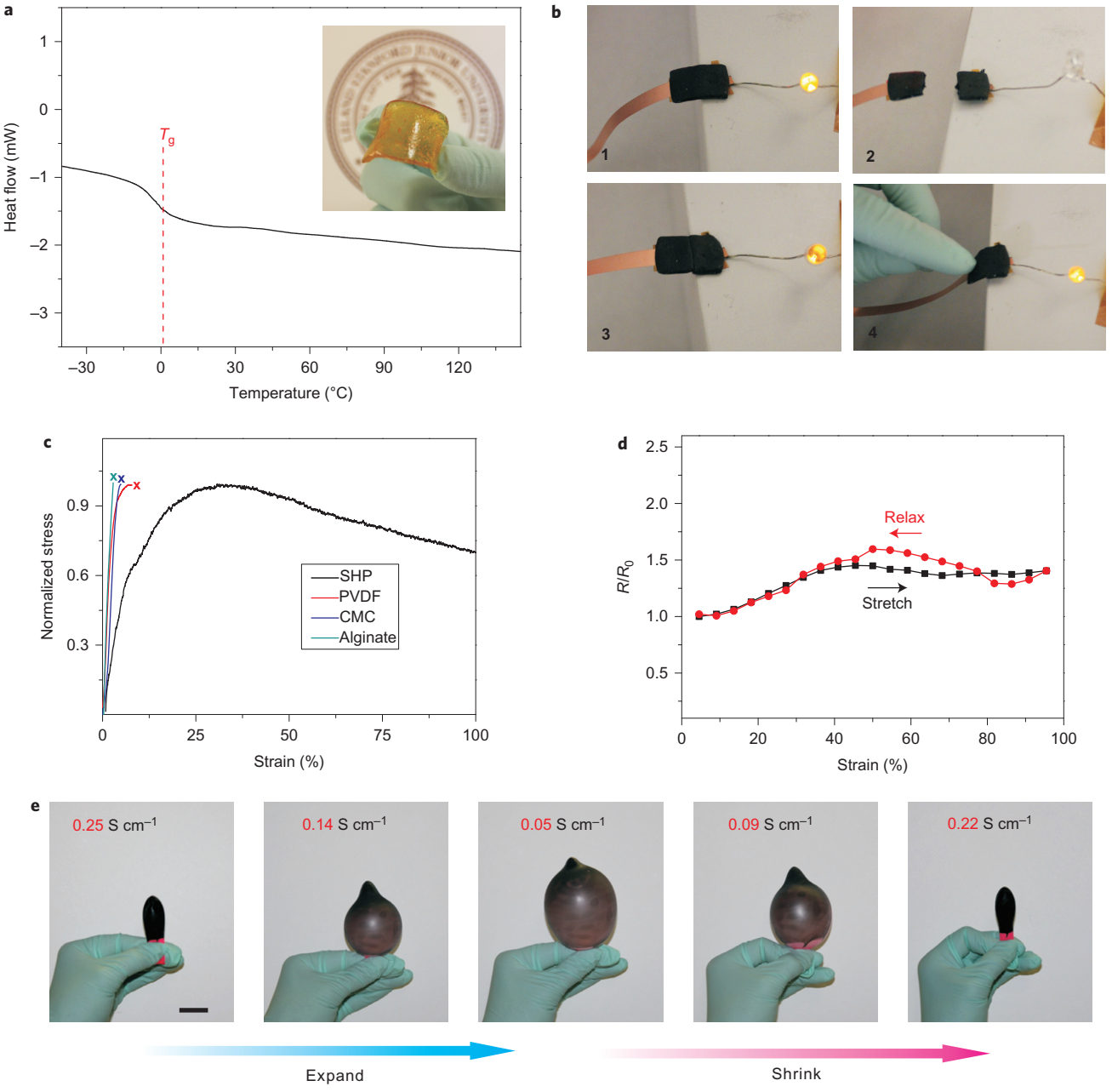


**Figure 2 | Characterization of the self-healing composite material. a**, DSC curve of the SHP showing that the $T_g$ of SHP is 0 °C, much lower than room temperature. Inset: photograph of the SHP. **b**, Demonstration of the electrical and mechanical self-healing capability of the conductive composite using a battery-powered circuit with the composite SHP as the conductive pathway that connects the LED to the battery. **c**, Tensile tests of the SHP and other conventional polymer binders show that SHP exhibits much higher stretchability than conventional polymer binders. **d**, The ratio between the resistance ($R$) and initial resistance ($R_0$) at different strains shows that the SHP/CB composite remains conductive over the whole stretching cycle. **e**, The SHP/CB composite material was coated onto an inflatable balloon to mimic the volumetric changes of silicon particles over the cycling process. The changes in its electrical conductivity during the balloon's repeated cycles of inflation and deflation were monitored. The SHP/CB coating remains conductive over the whole expand/shrink process. Scale bar, 2 cm.

drastic contrast to SiMP anodes with PVDF, CMC and alginate, which demonstrated poor stability and retained only 14%, 27% and 47%, respectively, of their initial capacities after 20 cycles at the same current density (0.4 A g$^{-1}$). The performances of SiMP electrodes with these conventional binders are consistent with those in many previous reports[41,45–47]. When defining the cycle life as the number of cycles to reach 80% of the initial capacity, the cycling lifetime of our self-healing SiMP electrode (90 cycles) is more than ten times longer than those of all the other SiMP electrodes (<9 cycles). The superior cycling stability and the high capacity of the SiMP/SHP/CB electrode are highly repeatable. We monitored the electrochemical cycling performance of six different batches of SiMP/SHP/CB electrodes and all of them showed a similar high capacity as well as a negligible capacity loss after 20 cycles of deep charge/discharge cycling (Fig. 3c). Furthermore, a control sample with the same electrode structure but without SHP (Supplementary Fig. 13) also showed poor cycling stability, which confirms that the good cycling performance arises because of the SHP.

Rate-capability tests showed that the SiMP/SHP/CB electrodes retain their stable cycling stability at various rates, as shown

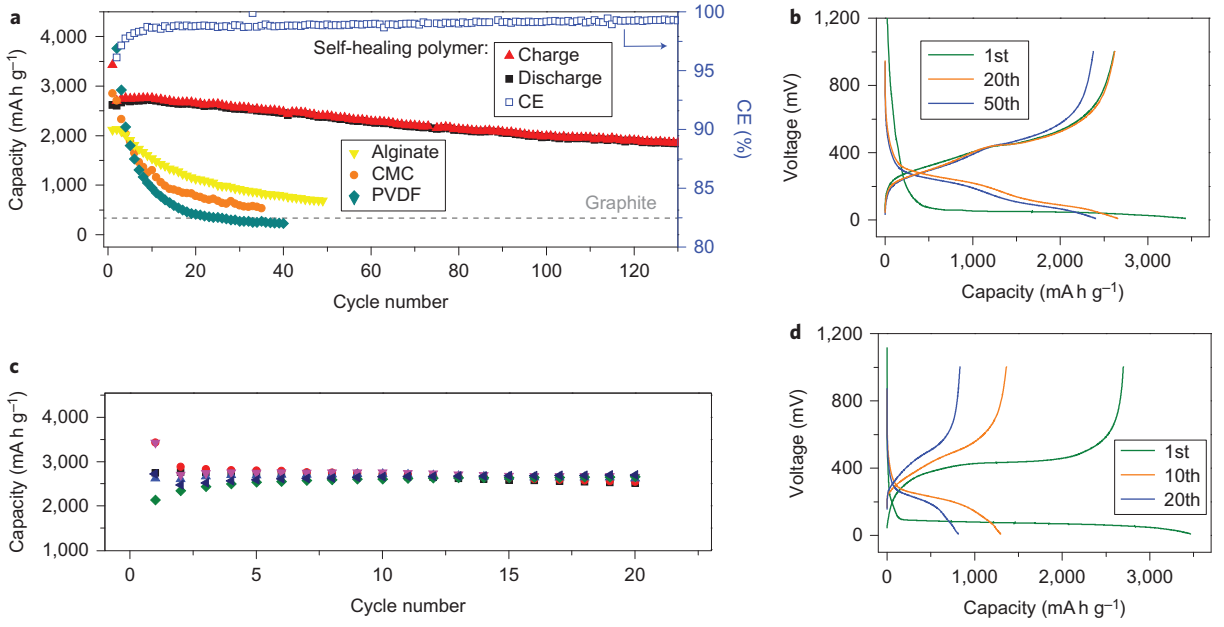


**Figure 3 | Electrochemical properties of SiMP electrodes. a**, Capacity retention of SiMP electrodes with different polymer additives, including the SHP/CB composite and conventional polymer binders (PVDF, CMC and alginate). All samples were cycled at the same charge/discharge rate of *C*/10 with a potential window of 0.01–1 V versus $Li/Li^+$. The grey dashed line indicates the theoretical capacity of a graphite electrode. The SiMP electrode with SHP showed a much longer cycling lifetime than that of conventional polymer binders. **b**, Voltage profiles of a SiMP/SHP/CB electrode at the first, 20th and 50th cycles, showing very little capacity decay during the cycling. **c**, Discharge capacity retention for six different SiMP/CMC electrode samples at a charging/discharging rate of *C*/10. All six different batches showed similar cycling performance. All the specific capacities are reported based on the weight of the SiMPs. **d**, Voltage profiles of a SiMP/CMC electrode at the first, 10th and 20th cycles show a much faster capacity decay than that of the self-healing electrode.

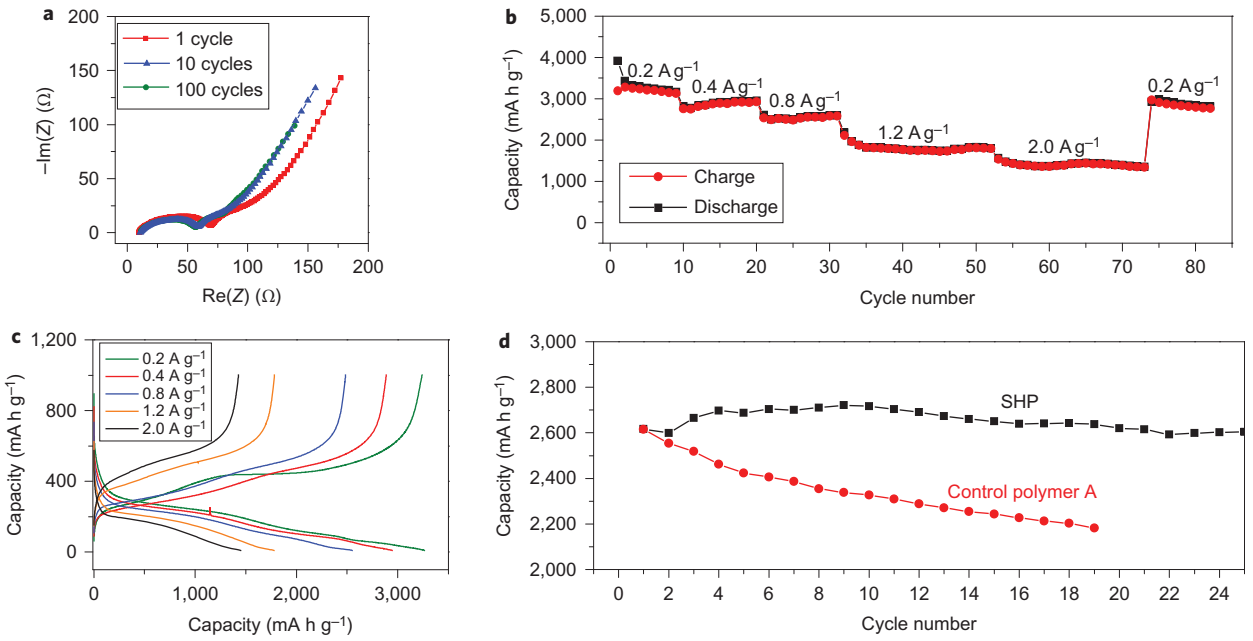


**Figure 4 | Cycling properties of the self-healing SiMP electrode. a**, Impedance spectroscopy measurements for a SiMP/SHP/CB electrode after different numbers of cycles, showing that no observable impedance increase even after 100 cycles. The real and imaginary parts of the complex impedance *Z* are denoted by Re(*Z*) and Im(*Z*), respectively. **b**,**c**, Capacity retention (**b**) and galvanostatic charge/discharge profiles (**c**) of a SiMP/SHP/CB electrode cycled at various current densities, showing the stable cycling stability at different charging/discharging rates. **d**, Discharge capacity retention of the SiMP electrode with SHP and control polymer A. Control polymer A showed much worse cycling stability than SHP. All samples were charged/discharged at a rate of *C*/10. All the specific capacities are reported based on the weight of the SiMPs.

in Fig. 4b,c. In addition, a high capacity of 3,200 mA h $g^{-1}$ was achieved at the charge/discharge current density of 0.2 A $g^{-1}$ (which corresponds to a cycling rate of *C*/20, where the rate was based on the theoretical capacity of silicon). The silicon mass loading was 0.5–0.7 mg $cm^{-2}$ and the areal capacity was about 1.5–2.1 mA h $cm^{-2}$ (Supplementary Fig. 14). Although further work is needed to meet the commercial requirement of lithium-ion batteries (3 mA h $cm^{-2}$), our areal capacity is much higher

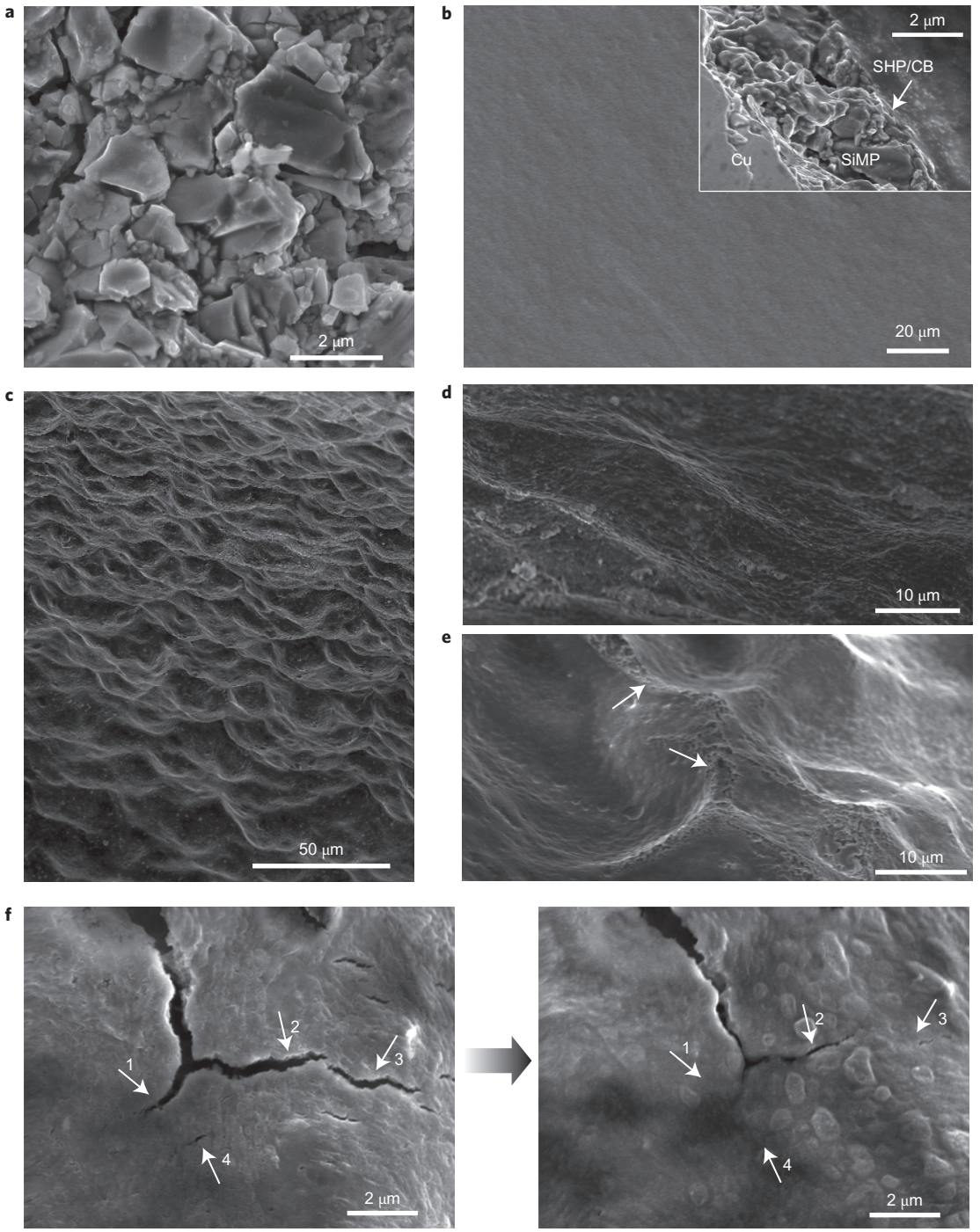


**Figure 5 | Structure of the self-healing SiMP electrode during electrochemical cycling. a**, Bare SiMPs have a large size distribution. The initial SiMPs have an average diameter of 4.2 μm, with a size-distribution range from 2 to 7 μm. **b**, Surface morphology of the electrode before cycling. Inset: cross-sectional SEM image of the electrode showing the layered structure. From left to right the layers are (1) a copper layer as the current collector, (2) the SiMP layer as the active material and (3) the self-healing conductive composite (SHP/CB) coating. **c**, A continuous wave-like morphology of the surface of the electrode is evident after 20 cycles at a rate of *C*/10. **d**, Magnified image of the wave-like structure. **e**, Some scar-like structures (arrows) can be found on the electrode after the cycling process, which appear to be cracks that subsequently healed. **f**, Left: cracks in the polymer layer in the lithiated state; right: after five hours the smaller cracks were healed, indicated by the arrows on the images.

than that of many other previous reports[25,26,28,29]. Even at a higher current density of 2.0 A $g^{-1}$ (or *C*/2 rate), the electrode was able to maintain a capacity of ~1,400 mA h $g^{-1}$ (Fig. 3f,g). Finally, the superior cycling stability of the SiMP/SHP/CB electrode was also observed in constant-capacity cycling experiments in which the lithium insertion capacity was limited to 1,000 mA h $g^{-1}$, with >500 electrode cycles (Supplementary Fig. 15).

Coulombic efficiency (CE) is also important for practical silicon-based electrodes[17,25]. For our SiMP/SHP/CB electrodes, the CE of the first cycle was more than 80%. In later cycles, the CE of the SiMP/SHP/CB electrode was about 98.5% at a cycling rate of *C*/10, and it reached 99.2% at a *C*/2 cycling rate. The CE of our SiMP electrode is comparable to those in previous reports on SiNPs and nanowires[26,27,29,33]. Our CE value indicates a relatively stable SEI formation

and minimal side reactions from the SHP in the electrode. In addition, no observable impedance increase occurred, even after 100 cycles, which indicates limited growth of the SEI during the cycling processes. However, our CE was still lower than the requirement for commercial lithium-ion batteries, but may be improved by surface treatments, electrolyte modifications[38] and using a micro-size silicon alloy[35,37] with less volume expansion.

**Mechanism studies.** The improved cycling stability of the electrode can be attributed to two major features associated with the SHP/CB composite coating: (1) stretchability and (2) spontaneous self-healing capabilities. Owing to its superior mechanical stretchability as well as its strong interactions with the silicon surface (Supplementary Fig. 16), the SHP/CB coating can better withstand the large volumetric changes of SiMPs during lithiation/delithiation to bring the shrunk and silicon particles into contact with the polymer binder and at the same time avoid large non-healable cracks in the polymer binder. When the SHP/CB composite coating does undergo fracture, it can proceed to self-heal. These two unique features of our SHP allow the electrode structure to be maintained over repeatable cycling processes. To provide further evidence, the morphology of the electrode with cycling was monitored using scanning electron microscopy (SEM). Before cycling, the SiMP layer (~3 μm) was covered with a thin layer (~200 nm) of the conductive SHP/CB composite, which displayed a flat and smooth morphology (Fig. 5a,b). After electrochemical cycling (20 cycles at a rate of *C*/10), the SHP/CB layer became rough and had a continuous wave-like morphology (Fig. 5c,d). This is caused by the underlying SiMPs being deformed when subjected to repeated volume expansion and contraction processes. No significant cracks or delaminations were observed. Cross-sectional SEM imaging of the electrode after cycling showed that a clear boundary still exists between the SHP/CB and SiMP layers, which indicates that the electrode structure is highly stable over the repeated cycling processes (Supplementary Fig. 18).

The self-healing capability of the electrode was also captured by SEM (Fig. 5f). Small cracks were, indeed, observed in the polymer coating on the lithiated and expanded silicon immediately after charging. However, when the sample was subsequently left for five hours, we observed that the initial smaller cracks were completely healed (indicated by the arrows). In addition, the larger cracks also showed partial healing, and they were able to heal more completely during the delithiation process because the shrinking process brought the fractured surfaces into closer contact.

The contribution of the self-healing effect to the battery performance was further confirmed by replacing SHP with control polymer A, which is also highly stretchable, but has significantly less self-healing capability than SHP (Supplementary Scheme 1 and Supplementary Fig. 16). Batteries made with control polymer A showed much lower cycling stability compared to those made with the SHP (Fig. 4d). Previous reports of fabricated silicon anodes with highly stretchable synthetic rubbers (for example, styrene–butadiene–rubber or PVDF–tetrafluoroethylene–propylene), but without self-healing ability, only show limited improvement in their cycling stability[48,49].

## Conclusion

In summary, we present here a successful demonstration of self-healing chemistry in battery application. Other alloy-type anode materials with large volume changes during cycling, such as tin and germanium, could potentially benefit from this approach, and it could possibly be advantageous for certain cathode materials, such as sulfur. Specifically, by modifying SiMPs into porous SiMPs or taking silicon alloys, which have higher structural stability, and combining these with the self-healing approach, we may be able to achieve stable silicon electrodes with an areal capacity that meets the requirement of commercial lithium-ion batteries. This new concept of a self-healing electrode may also be useful for other materials that suffer from mechanical issues during electrochemical reactions, including electrode materials for fuel cells, water splitting and catalysis.

## Methods

We synthesized SHP through a condensation reaction. The conductivity on stretching was tested using a home-made precision mechanical stretching system integrated with Keithley 4200. The stretching and releasing speed were both at 5 mm $min^{-1}$.

**Battery fabrication.** SHP (100 mg) was dissolved in chloroform (1 ml) and then mixed with CB material (15 mg (TIMCAL)) using a Dual Asymmetric Centrifugal Mixer (3,500 r.p.m., 135 seconds; Flacktek DAC 150.1 FVZ) to obtain a homogeneous suspension. The suspension was then drop-cast onto a glass slide and dried overnight to form the self-healing conductive composite. SiMP (0.1 g, ABCR) was dispersed in ethanol (10 ml) by sonication. Working electrodes were prepared by drop-casting the silicon suspension onto Cu foil (Fukuda). After drying at room temperature followed by calendaring, uniform electrodes with a SiMP loading of 0.5–0.7 mg $cm^{-2}$ were prepared. The weight ratio between silicon-active materials and polymer composite was 1:1. The area specific capacity was 1.5–2.1 mA h $cm^{-2}$. The silicon electrode was heated to 100 °C on a hot plate. The self-healing conductive composite was then melted at 100 °C and coated on the silicon electrode with a sharp blade. The electrodes were degassed in vacuum at room temperature overnight and transferred to an argon glove box for battery assembly. The electrochemical properties were examined by galvanostatic cycling of 2,032 stainless-steel coin cells with the SiMP/SHP/CB electrode as the working electrode. Lithium metal foil (1 mm thick) was used as a counter electrode. The electrolyte for all tests was 1 M $LiPF_6$ in ethylene carbonate/diethyl carbonate/fluoroethylene carbonate (1:1:0.04 vol/vol/vol (Ferro Corporation)), and separators (25 μm) from Asahi Kasei were used. All electrochemical measurements were carried out at room temperature in two-electrode 2,032 coin-type half-cells. The charge and discharge rates were calculated assuming theoretical capacities for silicon. The CE was calculated as $(C_{dealloy}/C_{alloy}) \times 100\%$, where $C_{alloy}$ and $C_{dealloy}$ are the capacity of the anodes for lithium insertion and extraction.

Received 18 August 2013; accepted 16 October 2013; published online 17 November 2013

## References


1. Bergman, S. D. & Wudl, F. Mendable polymers. *J. Mater. Chem.* **18,** 41–62 (2008).
2. White, S. R. *et al.* Autonomic healing of polymer composites. *Nature* **409,** 794–797 (2001).
3. Chen, X. *et al.* A thermally re-mendable cross-linked polymeric material. *Science* **295,** 1698–1702 (2002).
4. Ghosh, B. & Urban, M. W. Self-repairing oxetane-substituted chitosan polyurethane networks. *Science* **323,** 1458–1460 (2009).
5. Cordier, P., Tournilhac, F., Soulie-Ziakovic, C. & Leibler, L. Self-healing and thermoreversible rubber from supramolecular assembly. *Nature* **451,** 977–980 (2008).
6. Tee, B. C., Wang, C., Allen, R. & Bao, Z. An electrically and mechanically self-healing composite with pressure- and flexion-sensitive properties for electronic skin applications. *Nature Nanotechnol.* **7,** 825–832 (2012).
7. Burnworth, M. *et al.* Optically healable supramolecular polymers. *Nature* **472,** 334–337 (2011).
8. Chen, Y., Kushner, A. M., Williams, G. A. & Guan, Z. Multiphase design of autonomic self-healing thermoplastic elastomers. *Nature Chem.* **4,** 467–472 (2012).
9. Li, Y., Li, L. & Sun, J. Bioinspired self-healing superhydrophobic coatings. *Angew. Chem. Int. Ed.* **49,** 6129–6133 (2010).
10. Wong, T-S. *et al.* Bioinspired self-repairing slippery surfaces with pressure-stable omniphobicity. *Nature* **477,** 443–447 (2011).
11. Williams, K. A., Boydston, A. J. & Bielawski, C. W. Towards electrically conductive, self-healing materials. *J. Royal Soc. Interface* **4,** 359–362 (2007).
12. Blaiszik, B. J. *et al.* Autonomic restoration of electrical conductivity. *Adv. Mater.* **24,** 398–401 (2012).
13. Li, Y., Chen, S., Wu, M. & Sun, J. Polyelectrolyte multilayers impart healability to highly electrically conductive films. *Adv. Mater.* **24,** 4578–4582 (2012).
14. Palleau, E., Reece, S., Desai, S. C., Smith, M. E. & Dickey, M. D. Self-healing stretchable wires for reconfigurable circuit wiring and 3D microfluidics. *Adv. Mater.* **25,** 1589–1592 (2013).
15. Beaulieu, L. Y., Eberman, K. W., Turner, R. L., Krause, L. J. & Dahn, J. R. Colossal reversible volume changes in lithium alloys. *Electrochem. Solid-State Lett.* **4,** A137–A140 (2001).
16. Goodenough, J. B. & Kim, Y. Challenges for rechargeable Li batteries. *Chem. Mater.* **22,** 587–603 (2009).

17. Tarascon, J. M. & Armand, M. Issues and challenges facing rechargeable lithium batteries. *Nature* **414,** 359–367 (2001).
18. Cheng, Y-T. & Verbrugge, M. W. The influence of surface mechanics on diffusion induced stresses within spherical nanoparticles. *J. Appl. Phys.* **104,** 083521 (2008).
19. Besenhard, J. O., Yang, J. & Winter, M. Will advanced lithium-alloy anodes have a chance in lithium-ion batteries? *J. Power Sources* **68,** 87–90 (1997).
20. Kang, B. & Ceder, G. Battery materials for ultrafast charging and discharging. *Nature* **458,** 190–193 (2009).
21. Zhang, W. J. A review of the electrochemical performance of alloy anodes for lithium-ion batteries. *J. Power Sources* **196,** 13–24 (2011).
22. Arico, A. S., Bruce, P., Scrosati, B., Tarascon, J-M. & van Schalkwijk, W. Nanostructured materials for advanced energy conversion and storage devices. *Nature Mater.* **4,** 366–377 (2005).
23. Lee, Y. J. *et al.* Fabricating genetically engineered high-power lithium-ion batteries using multiple virus genes. *Science* **324,** 1051–1055 (2009).
24. Hatchard, T. D. & Dahn, J. R. *In situ* XRD and electrochemical study of the reaction of lithium with amorphous silicon. *J. Electrochem. Soc.* **151,** A838–A842 (2004).
25. Wu, H. *et al.* Stable cycling of double-walled silicon nanotube battery anodes through solid–electrolyte interphase control. *Nature Nanotechnol.* **7,** 309–314 (2012).
26. Chan, C. K. *et al.* High-performance lithium battery anodes using silicon nanowires. *Nature Nanotechnol.* **3,** 31–35 (2008).
27. Kovalenko, I. *et al.* A major constituent of brown algae for use in high-capacity Li-ion batteries. *Science* **333,** 75–79 (2011).
28. Liu, G. *et al.* Polymers with tailored electronic structure for high capacity lithium battery electrodes. *Adv. Mater.* **23,** 4679–4683 (2011).
29. Wu, H. & Cui, Y. Designing nanostructured Si anodes for high energy lithium ion batteries. *Nano Today* **7,** 414–429 (2012).
30. Guo, J. & Wang, C. A polymer scaffold binder structure for high capacity silicon anode of lithium-ion battery. *Chem. Commun.* **46,** 1428–1430 (2010).
31. Kim, H., Han, B., Choo, J. & Cho, J. Three-dimensional porous silicon particles for use in high-performance lithium secondary batteries. *Angew. Chem. Int. Ed.* **47,** 10151–10154 (2008).
32. Ryou, M-H. *et al.* Mussel-inspired adhesive binders for high-performance silicon nanoparticle anodes in lithium-ion batteries. *Adv. Mater.* **25,** 1571–1576 (2013).
33. Magasinski, A. *et al.* High-performance lithium-ion anodes using a hierarchical bottom-up approach. *Nature Mater.* **9,** 353–358 (2010).
34. Obrovac, M. N. & Krause, L. J. Reversible cycling of crystalline silicon powder. *J. Electrochem. Soc.* **154,** A103–A108 (2007).
35. Obrovac, M. N., Christensen, L., Le, D. B. & Dahn, J. R. Alloy design for lithium-ion battery anodes. *J. Electrochem. Soc.* **154,** A849–A855 (2007).
36. Chevrier, V. *et al.* in *30th International Battery Seminar: Primary and Secondary Batteries – Other Materials* Vol. 1, 579–611 (Curren Associates).
37. Chen, Z., Chevrier, V., Christensen, L. & Dahn, J. R. Design of amorphous alloy electrodes for Li-ion batteries: a big challenge. *Electrochem. Solid-State Lett.* **7,** A310–A314 (2004).
38. Kasavajjula, U., Wang, C. & Appleby, A. J. Nano- and bulk-silicon-based insertion anodes for lithium-ion secondary cells. *J. Power Sources* **163,** 1003–1039 (2007).
39. Liu, W. R. *et al.* Effect of electrode structure on performance of Si anode in Li-ion batteries: Si particle size and conductive additive. *J. Power Sources* **140,** 139–144 (2005).
40. Obrovac, M. N. & Krause, L. J. Reversible cycling of crystalline silicon powder. *J. Electrochem. Soc.* **154,** A103–A108 (2007).
41. Ryu, J. H., Kim, J. W., Sung, Y .E. & Oh, S. M. Failure modes of silicon powder negative electrode in lithium secondary batteries. *Electrochem. Solid-State Lett.* **7,** A306–A309 (2004).
42. Yi, R., Dai, F., Gordin, M. L., Chen, S. & Wang, D. Micro-sized Si–C composite with interconnected nanoscale building blocks as high-performance anodes for practical application in lithium-ion batteries. *Adv. Energy Mater.* **3,** 295–300 (2013).
43. Wang, L. *et al.* A new approach for the fabrication of an alternating multilayer film of poly(4-vinylpyridine) and poly(acrylic acid) based on hydrogen bonding. *Macromol. Rapid Commun.* **18,** 509–514 (1997).
44. Montarnal, D., Tournilhac, F. O., Hidalgo, M., Couturier, J-L. & Leibler, L. Versatile one-pot synthesis of supramolecular plastics and self-healing rubbers. *J. Am. Chem. Soc.* **131,** 7966–7967 (2009).
45. Lestriez, B., Bahri, S., Sandu, I., Roué, L. & Guyomard, D. On the binding mechanism of CMC in Si negative electrodes for Li-ion batteries. *Electrochem. Commun.* **9,** 2801–2806 (2007).
46. Szczech, J. R. & Jin, S. Nanostructured silicon for high capacity lithium battery anodes. *Energy Environ. Sci.* **4,** 56–72 (2011).
47. Saint, J. *et al.* Towards a fundamental understanding of the improved electrochemical performance of silicon–carbon composites. *Adv. Funct. Mater.* **17,** 1765–1774 (2007).
48. Chen, Z., Christensen, L. & Dahn, J. R. Comparison of PVDF and PVDF–TFE–P as binders for electrode materials showing large volume changes in lithium-ion batteries. *J. Electrochem. Soc.* **150,** A1073–A1078 (2003).
49. Liu, W-R., Yang, M-H., Wu, H-C., Chiao, S. M. & Wu, N-L. Enhanced cycle life of Si anode for Li-ion batteries by using modified elastomeric binder. *Electrochem. Solid-State Lett.* **8,** A100–A103 (2005).


## Acknowledgements

Y.C. and Z.B. acknowledge funding support from the Department of Energy, through the SLAC National Accelerator Laboratory LDRD project, under contract DE-AC02-76SF00515, and from the Precourt Institute for Energy at Stanford University.

## Author contributions

C.W., H.W., Y.C. and Z.B. conceived and designed the experiments. Y.C. and Z.B. directed the project. C.W. prepared the self-healing materials. H.W. and Z.C. performed the battery assembly and characterization experiments. All authors discussed and analysed the data. C.W., H.W. and M.T.M. co-wrote the first draft of the manuscript. All authors discussed the results and commented on the manuscript.

## Additional information

Supplementary information is available in the online version of the paper. Reprints and permissions information is available online at www.nature.com/reprints. Correspondence and requests for materials should be addressed to Y.C. and Z.B.

## Competing financial interests

The authors declare no competing financial interests.